Radiation Pattern and Polarization Reconfigurable Antenna Using Dielectric Liquid

Ren, Jian; Zhou, Zhao; Wei, Zhaohui; Yin, Yingzeng

Published in:
IEEE Transactions on Antennas and Propagation

Publication date:
2021

Document Version
Accepted author manuscript, peer reviewed version

Radiation Pattern and Polarization Reconfigurable Antenna Using Dielectric Liquid

Jian Ren, *Member*, *IEEE*, Zhao Zhou, Zhao Hui Wei, Hao Ming Ren, Zhe Chen, Ying Liu, *Senior Member*, *IEEE*, and Ying Zeng Yin, *Member*, *IEEE*

***Abstract*—A reconfigurable antenna with radiation pattern and polarization reconfiguration capabilities is investigated in this paper. The antenna consists of a central dielectric resonator antenna (DRA) and two parasitic DRAs made of a liquid solution with low dielectric loss. Utilizing the flowing of liquid, the existing of parasitic DRA can be changed to produce different patterns. An omnidirectional pattern can be realized when only the central DRA radiates, while a unidirectional pattern can be obtained using the parasitic DRAs. Furthermore, the polarization of the antenna with unidirectional radiation can be changed by forming different parasitic DRAs, which can be realized via liquid flowing. Based on this principle, three different radiation states, namely, omnidirectional radiation and unidirectional radiation with *x*- or *y*-polarization, can be obtained. To verify the design, a prototype of the antenna operating at 2.4 GHz was simulated, fabricated, and measured. The measurement results indicate that the antenna provides effective impedance matching over the band of interest as well as radiation pattern and polarization reconfiguration capabilities.**

***Index Terms*—Pattern reconfigurable antenna, polarization reconfigurable antenna, liquid antenna, dielectric resonator antenna.**

I. Introduction

Over the past decades, considerable progress has been made in wireless communication, which has had significant impacts on daily life. Compactness, low cost, multi-functionality, and high integration ability have become the main trends in wireless communication system design. Traditional systems utilize different antennas to meet the requirements of communication, navigation, sensing, and other functions. However, using multiple antennas in a single system substantially increases the size and cost, presenting new challenges. Consequently, reconfigurable antennas [1]–[3], whose operating features can be changed dynamically, have attracted considerable attention. Based on reconfigurable technology, antennas with functions of frequency changing [4]–[7], polarization manipulation [8, 9], and radiation pattern control [10, 11] have been realized. In particular, due to the appeal of high integration ability, the combination of multiple reconfigurable functions into a single antenna has been investigated extensively, leading to the development of frequency- and pattern-reconfigurable antennas [12]–[14], polarization- and pattern-reconfigurable antennas [15], and frequency- and polarization-reconfigurable antennas [16, 17]. To realize reconfiguration capabilities, electrically controlled p-i-n diodes are commonly used. These diodes have the advantages of low cost, high changing speed, and compact size, although the antenna efficiency may be decreased due to the diode insertion loss. Micro-electromechanical system-based switches, which can be electrically controlled, are also commonly used [18, 19], providing high speed and low insertion loss. New materials, such as liquid metal [20]–[22] and phase-changing materials [23, 24], have also been introduced into the design of reconfigurable antennas.

Recently, liquid-based reconfigurable antennas have attracted considerable attention. In [25, 26], the authors presented liquid-based frequency-reconfigurable antennas. By changing the volume of liquid in the antenna's substrate, the effective dielectric constant could be changed, altering the operating frequency of the antenna. Utilizing distilled water as the material, a frequency-reconfigurable dielectric resonator antenna (DRA) was investigated in [27]. As the dielectric loss of water at low frequency is low, this type of antenna is suitable for VHF and UHF applications. In [28], the authors described a monopole antenna in which ionized fluid was used as the conductive material. By changing the liquid tube length, frequency tunability was achieved. Compared with frequency reconfiguration, radiation pattern and polarization reconfiguration can change the power radiated by the antenna, which has great potential for use in various applications. In [29], by changing the operation mode of the liquid DRA between the $HEM_{11\delta}$ and $TM_{01\delta}$ modes, the authors investigated a pattern-reconfigurable antenna with omnidirectional and directional radiation patterns. Also using a DRA, a polarization-reconfigurable antenna was proposed [30]. Additionally, a circular beam-steering antenna using a liquid tube as a parasitic reflector was investigated [31]. Liquid-based antennas utilize the fluidity of liquid, and by changing the volume or shape of the liquid, different operating modes can be obtained. Utilizing a liquid with low dielectric loss and low cost provides these antennas with high efficiency, high power handing, and low cost, making liquid-based antennas popular topics in recent years.

In this paper, a liquid-based reconfigurable antenna with both pattern and polarization reconfiguration capabilities based on DRA is presented. The antenna consists of a center cylindrical DRA operating in $TM_{01\delta}$ mode and two parasitic cylindrical DRAs made of liquid, operating in $HEM_{11\delta}$ modes. To achieve different states, the functions of the parasitic DRAs beside the center DRA are changed by adjusting the flow of the liquid. When only the center DRA exists, an omnidirectional pattern can be obtained. In contrast, when one of the parasitic DRAs exists, unidirectional radiation can be realized, whose polarization depends on the location of the parasitic DRA. Using this working principle, different radiation patterns and polarization states can be realized. In this study, a dielectric material with $\varepsilon_r = 15$ was used for the center DRA, while ethyl acetate solution was employed as the liquid to form the parasitic DRAs. For verification, a prototype of the antenna operating at 2.4 GHz for WLAN applications was fabricated and measured. The working mechanism of the antenna was examined by performing a full-wave simulation, and the antenna characteristics, including the S-parameters, radiation patterns and antenna gain and efficiency, were measured.

Manuscript received XXXX. This work was supported in part by the National Natural Science Foundation of China under Grant No. 61901316. (Corresponding author: Yingzeng Yin.)

J. Ren, Z. Zhou, Z. H. Wei, H. M. Ren, Y. Liu and Y. Z. Yin are with the National Key Laboratory of Antennas and Microwave Technology, Xidian University, Xi'an, Shaanxi, 710071, P. R. China. (email: Ying Zeng Yin: yyzeng@mail.xidian.edu.cn).

Z. Chen is with Guangdong Provincial Mobile Terminal Microwave and Millimeter-Wave Antenna Engineering Research Center, College of Electronics and Information Engineering, Shenzhen University, Shenzhen, Guangdong 518060, P. R. China

Color versions of one or more of the figures in this communication are available online at http://ieeexplore.ieee.org.

Digital Object Identifier 10.1109/TAP..xxx.xxx

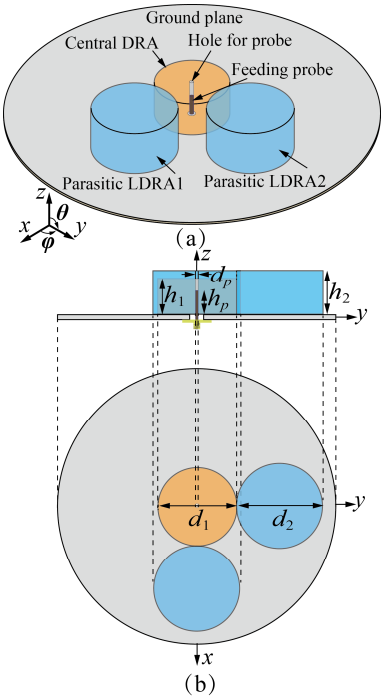

Fig. 1 (a) Diagram of the designed reconfigurable antenna. (b) Side and top views of the antenna. The following dimensions are marked: d_1 = 36 mm, d_2 = 42 mm, h_1 = 19 mm, h_2 = 23 mm, d_p = 1.27 mm, and h_p = 9 mm.

II. Antenna Configuration and Working Mechanism

Figure 1(a) depicts the designed reconfigurable antenna, which consists of a central DRA and two parasitic liquid DRAs (LDRA1 and LDRA2). For simplicity, the supporting structures are not shown. In practice, depending on the operation state, only one parasitic LDRA or no parasitic LDRA exists beside the central DRA. Figure 1(b) presents top and side views of the antenna, including the dimensions. The central DRA is cylindrical with diameter d_1 and height h_1. Located in the center of the ground plane, the central DRA is fed by a probe with diameter d_p and height h_p. Low-loss material, provided by Laird Technologies, with a dielectric constant ε_r of 15 forms the central DRA. To achieve pattern and polarization reconfiguration capabilities, ethyl acetate, a low-toxicity liquid with a dielectric constant e_{r2} of 6.6 [29], is used for the parasitic LDRAs. The parasitic LDRAs are also cylindrical with diameter d_2 and height h_2. By utilizing the fluidity of the liquid, the parasitic LDRAs can be formed beside the central DRA and act as parasitic radiators. When a different LDRA exists, different radiation characteristics can be obtained, as will be discussed in detail later. The whole antenna has a ground plane with diameter d_g of 80 mm. The working principle and radiation characteristics corresponding to different states are now discussed, as obtained by performing full wave simulations using ANSYS HFSS, which is based on the finite element method.

A. STATE1: Omnidirectional Radiation

In STATE1, only the central DRA exists, as shown in Fig. 2(a). Using the simulation software, the vector E- and H-fields in the meridian and equatorial planes of the DRA were obtained, as depicted in Fig. 2(b). With reference to the figure, we can see that the H-field is well contained in the resonator and forms a loop with constant magnitude in the azimuthal direction. The E- and H-field distributions clearly indicate that the $TM_{01\delta}$ mode is excited in this case. Figure 3 shows the simulated 3D radiation pattern of the antenna. These results clearly demonstrate that omnidirectional radiation was obtained.

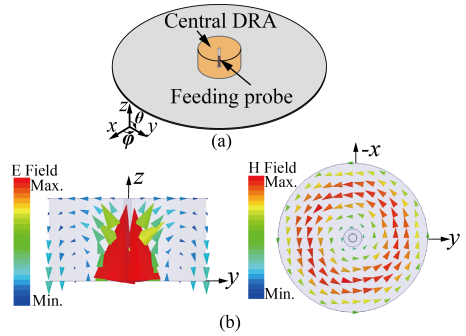

Fig. 2. (a) Diagram of the antenna operating in STATE1. No LDRA exists, and the central DRA acts as the radiator. (b) Simulated E- and H-fields in the meridian and equatorial planes of the DRA.

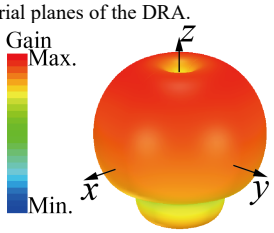

Fig. 3. Simulated 3D radiation pattern of the DRA in STATE1.

Given the frequency of 2.4 GHz and dielectric constant ε_r = 15, one can calculate the radius r and height h of the central DRA for the $TM_{01\delta}$ mode according to the operating frequency formula of a cylindrical DRA [32]:

$$f = 47.713 \times \frac{\sqrt{3.83^2+(\frac{\pi r}{2h})^2}}{a\sqrt{e_r+2}} \quad (1)$$

It should be noted that the structure presented here is different from that in [33], where a probe covered by a dielectric was used to feed four cylindrical DRAs, generating monopole-like radiation, and the small central dielectric rod only acted as a modified probe. In the present design, the central DRA acts not only as the feeding structure for the parasitic DRAs, but also as a DRA operating in its $TM_{01\delta}$ mode in STATE1.

B. STATE2: Unidirectional Radiation with x-Polarization

In STATE2 and STATE3, one of the parasitic LDRAs exists beside the central DRA. The parasitic LDRA is excited by the central DRA and acts as the radiator. Figure 4(a) illustrates the antenna producing directional radiation with x-polarization. In this case, the parasitic LDRA is located beside the central DRA, Fig. 4(b) and 4(c) illustrate the vector E- and H-fields in the meridian and equatorial planes of the antenna. For the H-field, the observation plane is located at $h_2/2$ above the ground plane. In this case, the fields of both the central DRA and LDRA are strong, indicating that the central DRA works as the radiator and feeding structure for the parasitic LDRA simultaneously. The magnetic field of the parasitic DRA shows a dipole-like distribution, and the polarization is along the y-axis. Meanwhile, the electric field of the parasitic LDRA shows a half-circular distribution. Thus, it can be said that the $HEM_{11\delta}$ mode of the cylindrical DRA is excited in the parasitic LDRA. The dimensions of the parasitic LDRA can be calculated using the mode formula with a given frequency and dielectric constant according to the operating frequency formula of $HEM_{11\delta}$ [32]:

$$f = \frac{6.324}{\sqrt{e_r+2}} \times (0.27 + 0.36\frac{r}{2h}) + 0.02(\frac{r}{2h})^2 \quad (2)$$

where r is the radius of the cylindrical DRA, h is the height of the DRA and e_r is the dielectric of the used material. As the $TM_{01\delta}$ and $HEM_{11\delta}$ modes are excited simultaneously, the radiation pattern is a combination of these two modes, with a certain spatial displacement.

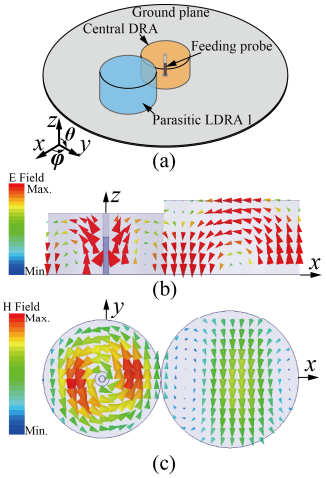

Fig. 4. (a) Diagram of the antenna operating in STATE2. LDRA1 exists, and the central DRA acts as the radiator and feeds LDRA1. (b) Simulated E-field in meridian plane of the antenna. (c) Simulated H-field in equatorial plane of the antenna.

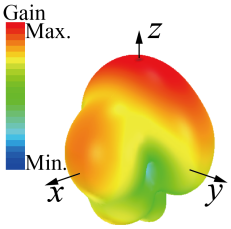

Fig. 5. Simulated 3D radiation pattern of the DRA in STATE2.

For the $HEM_{11\delta}$ mode, unidirectional radiation with *x*-polarization can be obtained and the maximum radiation direction is along the *z*-axis. Meanwhile, for the $TM_{01\delta}$ mode, omnidirectional radiation can be obtained and there are both *x*- and *y*-components, which increases the cross-polarization of the whole antenna. Accordingly, the initial dimensions of the parasitic LDRA obtained from (2) were optimized towards the objective of achieving low cross-polarization. It should be noted that although the size of the LDRA is changed, it can still operate in its $HEM_{11\delta}$ mode as the bandwidth of the mode is not narrow. Figure 5 shows the simulated 3D radiation pattern of the LDRA with the optimized size. Unidirectional radiation with *x*-polarization is clearly observable. The maximum value of the realized gain in this case is about 6.32 dBi.

C. STATE3: Unidirectional Radiation with y-Polarization

When LDRA1 is moved and LDRA2 exists beside the central DRA, unidirectional radiation with *y*-polarization is obtained. The antenna's configuration for this case is shown in Fig. 6(a). As the working principle of this state is the same as that of STATE2, only the simulated 3D radiation pattern of the antenna is shown (Fig. 6(b)). Compared with STATE2, only the location of the parasitic LDRA differs, so the shapes of the radiation patterns are quite similar despite their 90° displacement along the *z*-axis. As the parasitic DRA is the main radiator in this state, the antenna has a unidirectional pattern with *y*-polarization. The maximum value of the antenna gain in this case is also about 6.32 dBi.

III. Fabrication and Measurement

Based on the above discussion, the antenna has three different radiation states corresponding to different states of the parasitic LDRAs: omnidirectional radiation and unidirectional radiation with *x*- or *y*-polarization. In practice, the different antenna states are obtained by controlling the flow of the liquid to form different LDRAs. Different kinds of liquid, such as water [34] and oil [26], have been used in reconfigurable antenna designs. In the developed system, ethyl acetate is used to obtain a high radiation efficiency. This material has a dielectric constant of 6.6, as measured using an Agilent 85070D system [29]. Further, ethyl acetate is a low-cost solution with low toxicity. To contain the liquid, two containers fabricated using 3D printing technology are employed. Photosensitive resin with a dielectric constant of approximately 2.7 and loss tangent of 0.02 is employed as the printing material. Although the dielectric loss of the printing material is not low, the energy is mainly distributed in the DRA and an acceptable radiation efficiency can be obtained. Figures 7(a) and 7(b) depict the prototype of the fabricated liquid container, and Fig. 7(c) shows an exploded view of the whole antenna structure, including the central DRA, liquid containers for LDRA1 and LDRA2, feeding probe of the antenna, and ground plane. In addition, two circular grooves are etched on the ground plane so that the walls of the containers can be inserted into the grooves to avoid liquid leakage.

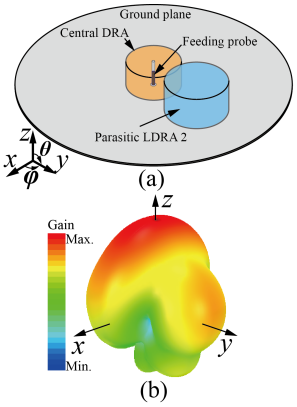

Fig. 6. (a) Diagram of the antenna operating in STATE3. LDRA2 exists, and the central DRA acts as the radiator and feeds LDRA2. (b) Simulated 3D radiation pattern of the DRA for STATE3.

Control of the liquid is an important issue in this design. Figure 8(a) illustrates the liquid control system used in this antenna. The liquid control system contains a liquid reservoir, two pumps, and four pairs of injection/outlet pipes. Each pair of pipes includes a longer one for air injection/outlet and a shorter one for liquid injection/outlet. The liquid reservoir is placed beneath the ground plane to preserve extra liquid. Through the two pairs of injection/outlet pipes inside the liquid reservoir, the reservoir is connected to two pumps. These pumps are connected to the injection/outlet pipes in the LDRA1 and LDRA2 containers, respectively. Driven by the pumps, the liquid can be transferred between the LDRA containers and reservoir to generate different working states. During the process of the liquid filling, there may be some bubbles with quite small size at the top part of the container. As the volume of the air is incomparable to that of the liquid, the effect of the bubbles on the performance of the antenna is negligible. The pumping speed is set as 30 *ml/min* and with this speed, it costs about 1 minute to pump the liquid into the container. Note that a single reservoir serves both LDRA containers simultaneously. Considering that all of the aforementioned working states involve no more than one LDRA, a single reservoir can certainly meet the requirements of this liquid control system. Also, it is noted that two pumps with single channels is used to control the liquid. The commercially available pumps with two separate channels can be used here to reduce the complexity of the control system, which may increase the cost of the antenna.

For verification, a prototype of the antenna with the optimal parameters was fabricated and measured, as depicted in Fig. 8(b). The S parameters of the antenna were obtained using the Keysight vector

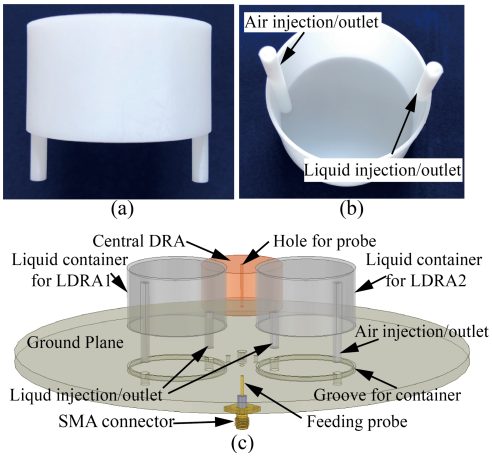

Fig. 7. (a) Side view and (b) Back view of the prototype container. (c) Exploded view of the whole antenna structure.

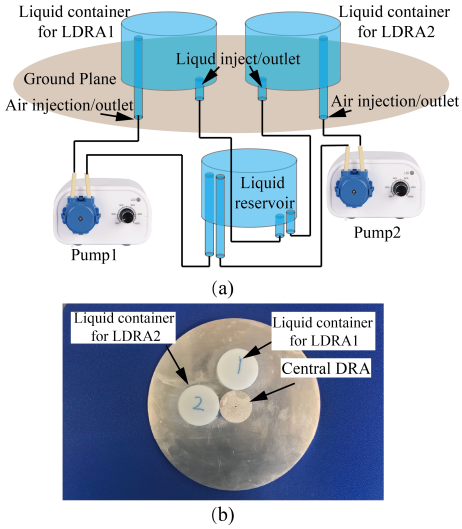

Fig. 8. (a) Illustration of the liquid control system for the antenna. (b) Prototype of the proposed antenna.

network analyzer 8753, while the near-field radiation measurement system Satimo StarLab provided by Microwave Vision Group was used to obtain the far-field characteristics of the antenna, including the radiation pattern, antenna gain, and radiation efficiency. During the measurement, all of the antenna structure and control system of the liquid was included in the chamber. During the measurement, the control system would not work. As there are metal structure in the pump, the liquid control system may have a little effect on the performance of the antenna, mainly on the antenna radiation pattern at the back direction. To avoid the effect, we placed the control system a distance to the antenna and the liquid was injected through a long tube. In this case, the effect can be minimized.

A. Reflection Coefficient

Figure 9 shows the simulated and measured reflection coefficients of the antenna corresponding to different states. With reference to the figure, we can see that the simulation and measurement results agree well in all of the investigated states. For STATE1, the impedance bandwidth can cover 2.35–3 GHz, with a relative bandwidth wider than 22.9%. For STATE2 and STATE3, the antenna has a wide bandwidth around 23%, which can cover 2.34–2.95 GHz. The bandwidth overlap of the different states can fully cover the 2.4 GHz WLAN band (2.4–2.48 GHz).

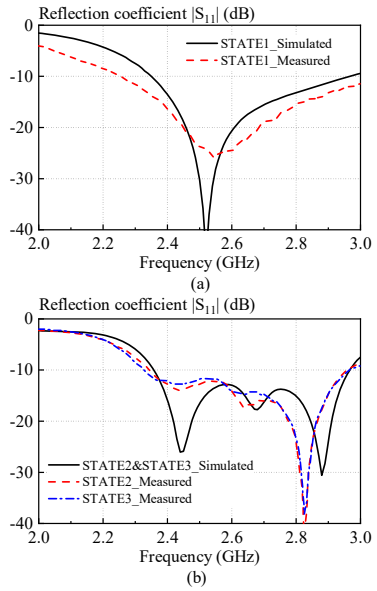

Fig. 9. Simulated and measured reflection coefficients of the proposed antenna. (a) STATE1. (b) STATE2 and STATE3.

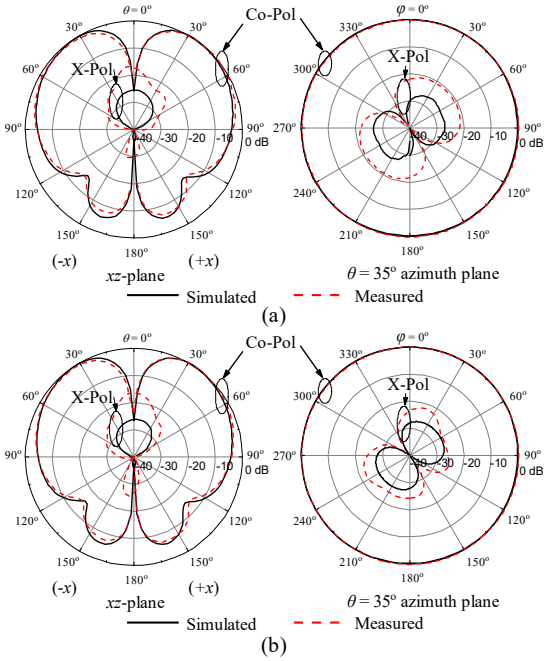

Fig. 10. Simulated and measured radiation patterns in different planes in STATE1. (a) f = 2.4 GHz. (b) f = 2.5 GHz.

B. Radiation Pattern

Using the Satimo StarLab near-field measurement system, the radiation patterns of the different antenna states were obtained. As the antenna is designed for 2.4 GHz WLAN, the radiation patterns corresponding to 2.4 GHz and 2.5 GHz are presented here. Figure 10 shows the omnidirectional radiation corresponding to $TM_{01\delta}$ mode, together with the simulated radiation pattern for comparison. The simulation and measurement results agree well at both frequencies. A radiation null in the boresight direction can be found in the elevation plane (*xoz* plane). The maximum radiation occurs at approximately θ = 35°. In the azimuthal plane (θ = 35°), the antenna produces omnidirectional radiation. As the cylindrical DRA is the central antenna, the pattern variation in the azimuthal plane is less than 0.3 dB, despite the existence of liquid containers for LDRA1 and LDRA2.

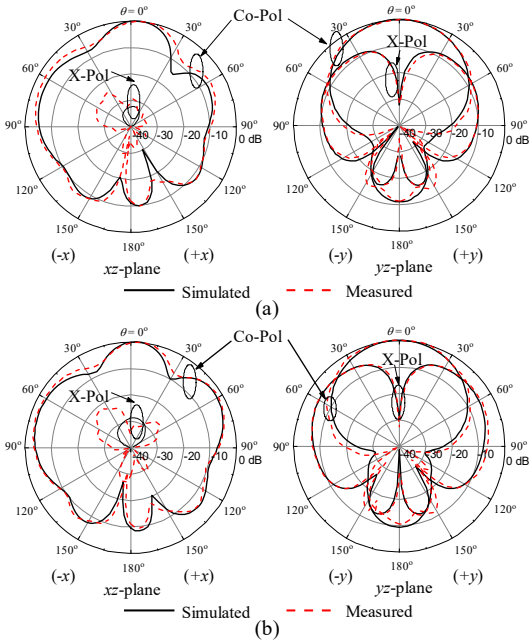

Fig. 11. Simulated and measured radiation patterns in different planes in STATE2. (a) f = 2.4 GHz. (b) f = 2.5 GHz.

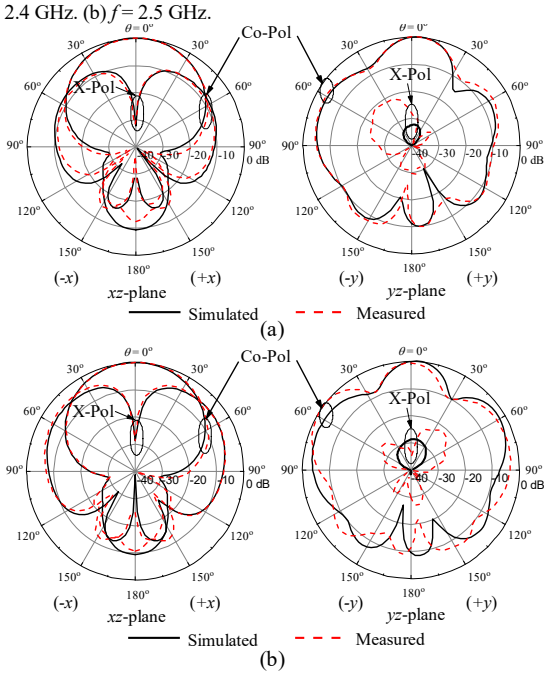

Fig. 12. Simulated and measured radiation patterns in different planes in STATE3. (a) f = 2.4 GHz. (b) f = 2.5 GHz.

Figure 11 shows the simulated and measured radiation patterns in the E-plane (*xoz* plane) and H-plane (*yoz* plane) of the antenna in STATE2. The simulation and measurement results agree well at all of the investigated frequencies. Unidirectional, *x*-polarized radiation is clearly observable. For the E-plane (*xoz* plane), a small tilt angle is evident as the antenna is asymmetric in this plane. A cross-polarization level as low as -20 dB is obtained. For the radiation in the H-plane (*yoz* plane), the maximum direction is the boresight direction (θ = 0°). As the antenna structure is symmetric in the *yoz* plane, the radiation patterns for co- and cross-polarization are symmetric. In the boresight direction, the cross-polarization level is lower than –20 dB, and in the other directions, the cross-polarization increases as θ increases. This trend occurs because in the boresight direction, the radiation of the HEM mode dominates, while the power radiated by the TM mode can be ignored. Further, the antenna has higher cross-polarization at higher frequency, because in this case, the total radiation of the antenna is the combination of the TM and HEM modes. As discussed in Section II, the cross-polarization was optimized by choosing the properties of the parasitic DRA at 2.4 GHz. As the frequency increases, the cross-polarization may increase slightly. Ultimately, unidirectional, *x*-polarized radiation is obtained. Also, it can be seen that the sidelobe of the antenna in *xoz* plane is not quite low. This can be explained by the electric field distribution in the antenna, as shown in Fig. 4(c). The field is like that of the higher order mode, making the sidelobe high. The sidelobe also can be suppressed by optimizing the size of the LDRA.

The simulated and measured radiation patterns of the antenna corresponding to unidirectional radiation with *y*-polarization are shown in Fig. 12. The radiation patterns are quite similar to those in STATE2 except that the antenna has different polarization. Reasonable agreement between the simulation and measurement results is observable.

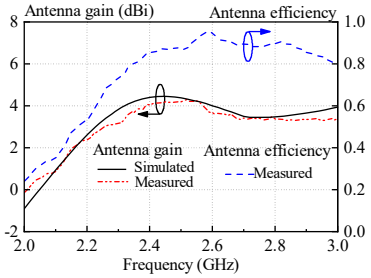

Fig. 13. Simulated and measured antenna gain and measured antenna efficiency in STATE1.

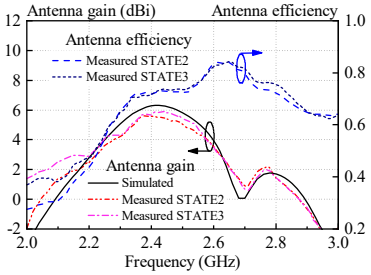

Fig. 14. Simulated and measured antenna gains in STATE2 and STATE3.

C. *Antenna Gain and Efficiency*

Figure 13 shows the simulated and measured antenna gain in STATE1, where the maximum gain of 4.2 dBi occurs at approximately 2.4 GHz. Over the entire operation band from 2.4 GHz to 2.48 GHz, the average antenna gain is around 4.1 dBi. The simulation and measurement results agree well over the entire band, with the measured values slightly lower than the simulated ones. The measured total efficiency of the antenna is also shown in Fig. 13. Over the entire operation band, the efficiency is higher than 85%, and the peak value occurs at approximately 2.6 GHz. Considering that the radiator for STATE1, the central DRA, is composed of material with extremely low dielectric loss and that the main loss originates from the material of the LDRA1 and LDRA2 containers, the high total efficiency of the antenna is reasonable.

Figure 14 shows the simulated and measured antenna gains and total efficiencies for STATE2 and STATE3. Again, the simulation and measurement results agree well. Note that the antenna gains depicted are those obtained in the boresight direction. Over the operation band, the antenna gain is higher than 5.3 dBi and the measured values are approximately 0.5–0.7 dB lower than the simulated ones. The maximum antenna gains occur at approximately 2.4 GHz, as expected. The total efficiencies are greater than 70% over the entire operation band. As the

liquid and central DRAs radiate simultaneously in this case, the loss of the LDRA is acceptable despite the high dielectric loss of the liquid used. It is worth mentioning that the efficiency of the proposed antenna is generally higher than those of the antennas proposed in [29], where the same liquid and DRA mode were used. The antenna gain and efficiency can be further increased by using a liquid with lower dielectric loss. In short, the obtained antenna gain and efficiency demonstrate the good radiation performance of the proposed antenna.

IV. Conclusion

In this study, we investigated an antenna with radiation pattern and polarization reconfiguration capabilities. The antenna consists of a central DRA and two parasitic DRAs of ethyl acetate. The antenna can be reconfigured by utilizing the flow of the liquid. When only the central DRA exists, the antenna operates in its $TM_{01\delta}$ mode, generating omnidirectional radiation. When one of the parasitic LDRAs exists in addition to the central DRA, the antenna emits unidirectional radiation, and the polarization depends on the location of the parasitic LDRA. The radiation characteristics can be changed via liquid flow, and three states can be realized: omnidirectional radiation and unidirectional radiation with *x*- and *y*-polarization. For verification, a prototype antenna operating at 2.4 GHz was simulated, fabricated, and measured. The simulation and measurement results agreed well. The measurement results indicated that the antenna provides good impedance matching for all three states over the entire band of interest and that the antenna radiation can be reconfigured. As expected, different radiation states were obtained, and reasonable gain and efficiency were achieved. For demonstration, here only two LDRAs are used to obtain radiation pattern and polarization reconfigurable capability. More LDRAs can be introduced into the antenna to obtain additional operation states, such as the unidirectional radiation with ±45°polarizations.

References

[1] C. G. Christodoulou, Y. Tawk, S. A. Lane, and S. R. Erwin, "Reconfigurable antennas for wireless and space applications," *Proc. IEEE,* vol. 100, no. 7, pp. 2250–2261, Jul. 2012.

[2] J. Costantine, Y. Tawk, S. E. Barbin, and C. G. Christodoulou, "Reconfigurable antennas: Design and applications," *Proc. IEEE,* vol. 103, no. 3, pp. 424–437, Mar. 2015.

[3] R. L. Haupt, and M. Lanagan, "Reconfigurable antennas," *IEEE Antennas Propag. Mag.,* vol. 55, no. 1, pp. 49–61, Feb. 2013.

[4] E. Erdil, K. Topalli, M. Unlu, O. A. Civi, and T. Akin, "Frequency tunable microstrip patch antenna using rf mems technology," *IEEE Trans. Antennas Propag.,* vol. 55, no. 4, pp. 1193–1196, Apr. 2007.

[5] L. A. Bronckers, A. Roc'h, and A. B. Smolders, "A new design method for frequency-reconfigurable antennas using multiple tuning components," *IEEE Trans. Antennas Propag.,* vol. 67, no. 12, pp. 7285–7295, Dec. 2019.

[6] M. Ikram, E. A. Abbas, N. Nguyen-Trong, K. H. Sayidmarie, and A. Abbosh, "Integrated frequency-reconfigurable slot antenna and connected slot antenna array for 4G and 5G mobile handsets," *IEEE Trans. Antennas Propag.,* vol. 67, no. 12, pp. 7225–7233, Dec. 2019.

[7] J. Liu, J. Li, R. Xu, and S. Zhou, "A reconfigurable printed antenna with frequency and polarization diversity based on bow-tie dipole structure," *IEEE Trans. Antennas Propag.,* vol. 67, no. 12, pp. 7628–7632, Dec. 2019.

[8] H. L. Zhu, S. W. Cheung, X. H. Liu, and T. I. Yuk, "Design of polarization reconfigurable antenna using metasurface," *IEEE Trans. Antennas Propag.,* vol. 62, no. 6, pp. 2891–2898, Jun., 2014.

[9] P. Qin, A. R. Weily, Y. J. Guo, and C. Liang, "Polarization reconfigurable U-slot patch antenna," *IEEE Trans. Antennas Propag.,* vol. 58, no. 10, pp. 3383–3388, Oct. 2010.

[10] J. Chang won, L. Ming-jer, G. P. Li, and F. D. Flaviis, "Reconfigurable scan-beam single-arm spiral antenna integrated with RF-MEMS switches," *IEEE Trans. Antennas Propag.,* vol. 54, no. 2, pp. 455–463, Feb. 2006.

[11] G. Jin, D. Liu, M. Li, and Y. Cui, "A pattern reconfigurable antenna with broadband circular polarization," *IEICE Transactions on Communications,* vol. E101B, no. 5, pp. 1257–1261, May. 2018.

[12] P. K. Li, Z. H. Shao, Q. Wang, and Y. J. Cheng, "Frequency- and pattern-reconfigurable antenna for multistandard wireless applications," *IEEE Antennas Wirel. Propag. Lett.,* vol. 14, pp. 333–336, 2015.

[13] H. A. Majid, M. K. A. Rahim, M. R. Hamid, and M. F. Ismail, "Frequency and pattern reconfigurable slot antenna," *IEEE Trans. Antennas Propag.,* vol. 62, no. 10, pp. 5339–5343, Oct. 2014.

[14] S. N. M. Zainarry, N. Nguyen-Trong, and C. Fumeaux, "A frequency- and pattern-reconfigurable two-element array antenna," *IEEE Antennas Wirel. Propag. Lett.,* vol. 17, no. 4, pp. 617–620, 2018.

[15] X. Yi, L. Huitema, and H. Wong, "Polarization and pattern reconfigurable cuboid quadrifilar helical antenna," *IEEE Trans. Antennas Propag.,* vol. 66, no. 6, pp. 2707–2715, Jun. 2018.

[16] P. Qin, Y. J. Guo, Y. Cai, E. Dutkiewicz, and C. Liang, "A reconfigurable antenna with frequency and polarization agility," *IEEE Antennas Wirel. Propag. Lett.,* vol. 10, pp. 1373–1376, 2011.

[17] N. Nguyen-Trong, A. Piotrowski, L. Hall, and C. Fumeaux, "A frequency- and polarization-reconfigurable circular cavity antenna," *IEEE Antennas Wirel. Propag. Lett.,* vol. 16, pp. 999–1002, 2017.

[18] G. M. Rebeiz *et al.*, "Tuning in to RF MEMS," *IEEE Microw. Mag.,* vol. 10, no. 6, pp. 55–72, Jun. 2009.

[19] H. J. D. L. Santos, G. Fischer, H. A. C. Tilmans, and J. T. M. v. Beek, "RF MEMS for ubiquitous wireless connectivity. Part II. Application," *IEEE Microw. Mag.,* vol. 5, no. 4, pp. 50–65, Apr. 2004.

[20] Z. Chen, H. Wong, and J. Kelly, "A polarization-reconfigurable glass dielectric resonator antenna using liquid metal," *IEEE Trans. Antennas Propag.,* vol. 67, no. 5, pp. 3427–3432, May. 2019.

[21] D. Rodrigo, L. Jofre, and B. A. Cetiner, "Circular beam-steering reconfigurable antenna with liquid metal parasitics," *IEEE Trans. Antennas Propag.,* vol. 60, no. 4, pp. 1796–1802, Apr. 2012.

[22] L. Song, W. Gao, C. O. Chui, and Y. Rahmat-Samii, "Wideband frequency reconfigurable patch antenna with switchable slots based on liquid metal and 3-D printed microfluidics," *IEEE Trans. Antennas Propag.,* vol. 67, no. 5, pp. 2886–2895, May. 2019.

[23] B. Gerislioglu, A. Ahmadivand, M. Karabiyik, R. Sinha, and N. Pala, "VO2-based reconfigurable antenna platform with addressable microheater matrix," *Adv. Electron. Mater.,* vol. 3, no. 9, 1700170, Sep. 2017.

[24] T. S. Teeslink, D. Torres, J. L. Ebel, N. Sepulveda, and D. E. Anagnostou, "Reconfigurable bowtie antenna using metal-insulator transition in vanadium dioxide," *IEEE Antennas Wirel. Propag. Lett.,* vol. 14, pp. 1381-1384, 2015.

[25] M. Konca, and P. A. Warr, "A frequency-reconfigurable antenna architecture using dielectric fluids," *IEEE Trans. Antennas Propag.,* vol. 63, no. 12, pp. 5280-5286, Dec. 2015.

[26] S. Wang, L. Zhu, and W. Wu, "A novel frequency-reconfigurable patch antenna using low-loss transformer oil," *IEEE Trans. Antennas Propag.,* vol. 65, no. 12, pp. 7316–7321, Dec. 2017.

[27] L. Xing *et al.*, "A high-efficiency wideband frequency-reconfigurable water antenna with a liquid control system: Usage for VHF and UHF applications," *IEEE Antennas Propag. Mag.*, to be published.

[28] C. Borda-Fortuny, L. Cai, K. F. Tong, and K.-K. Wong, "Low-cost 3D-printed coupling-fed frequency agile fluidic monopole antenna system," *IEEE Access,* vol. 7, pp. 95058–95064, 2019.

[29] Z. Chen, and H. Wong, "Wideband glass and liquid cylindrical dielectric resonator antenna for pattern reconfigurable design," *IEEE Trans. Antennas Propag.,* vol. 65, no. 5, pp. 2157–2164, May. 2017.

[30] Z. Chen, and H. Wong, "Liquid dielectric resonator antenna with circular polarization reconfigurability," *IEEE Trans. Antennas Propag.,* vol. 66, no. 1, pp. 444–449, Jan. 2018.

[31] L. Xing, J. Zhu, Q. Xu, D. Yan, and Y. Zhao, "A circular beam-steering antenna with parasitic water reflectors," *IEEE Antennas Wirel. Propag. Lett.,* vol. 18, no. 10, pp. 2140–2144, Oct. 2019.

[32] A. Petosa, *Dielectric resonator antenna handbook*: Artech House Publishers, 2007.

[33] D. Guha, and Y. M. M. Antar, "Four-element cylindrical dielectric resonator antenna for wideband monopole-like radiation," *IEEE Trans. Antennas Propag.,* vol. 54, no. 9, pp. 2657–2662, Sep. 2006.

[34] J. Sun, and K.-M. Luk, "A compact-size wideband optically-transparent water patch antenna incorporating an annular water ring," *IEEE Access,* vol. 7, pp. 122964–122971, 2019.